INTERNATIONAL JOURNAL OF HYDROGEN ENERGY 39 (2014) 8138–8146

Available online at www.sciencedirect.com

ScienceDirect

journal homepage: www.elsevier.com/locate/he

A numerical investigation on combustion characteristics of H_2/air mixture in a micro-combustor with wall cavities

Jianlong Wan [a], Wei Yang [a], Aiwu Fan [a,*], Yi Liu [a], Hong Yao [a], Wei Liu [a], Yiqing Du [a], Daiqing Zhao [b]

[a] State Key Laboratory of Coal Combustion, Huazhong University of Science and Technology, Wuhan 430074, China
[b] Guangzhou Institute of Energy Conversion, CAS, Guangzhou 510640, China

ARTICLE INFO

Article history:
Received 19 October 2013
Received in revised form
1 March 2014
Accepted 17 March 2014
Available online 16 April 2014

Keywords:
Micro combustion
Cavity
Length–depth ratio
Flame-splitting limit
Recirculation zone

ABSTRACT

Combustion characteristics of H_2/air mixture in a micro-combustor with wall cavities were investigated numerically. The effects of inlet velocity, equivalence ratio, and the length–depth ratio of the cavity were studied. The results show that at a high enough velocity the flame splits in the middle which leads to a large amount of fuel leakage and a sharp decrease in the conversion rate of hydrogen. Meanwhile, the flame splits at the inner wall which gives rise to two high temperature regions and double temperature peaks at outer wall. Moreover, the flame-splitting limit is extended at a higher equivalence ratio due to a more intensive reaction. Furthermore, the flame-splitting limit increases for a larger length–depth ratio of the cavity, whereas the wall temperature level decreases. Therefore, excessive large length–depth ratios are not beneficial for this type of micro-combustors if the combustor walls are used as heat sources of thermoelectric or thermal photovoltaic devices.

Introduction

With the rapid progresses of MEMS (Micro-Electro-Mechanic Systems) technology, various micro- and meso-scale devices and systems, including micro turbines, robots, satellites and portable electric devices, are continuously emerging. Because the electrochemical batteries have some disadvantages such as short life spans, long recharging periods and low energy densities, combustion-based micro-power-generation devices are considered to be potential alternatives due to the much higher energy densities of hydrocarbon fuels compared to batteries [1–3]. The micro-combustor is an important component in which the chemical energy of hydrocarbon is converted into thermal energy via combustion. Therefore, the development of micro-combustors with a wide operation range has attracted increasing attention during past few years.

However, there are some challenges to maintain stable combustion in micro combustors. Firstly, the increased heat losses and wall radical capture due to large surface area-to-volume ratio makes it difficult to sustain a stable flame under small scales [1–6]. Another critical problem is the shortened residence time of the fuel/oxidant mixture in the combustor. Up to now, many fantastic flames have been

* *Corresponding author*. State Key Laboratory of Coal Combustion, Huazhong University of Science and Technology, 1037 Luoyu Road, Wuhan 430074, China. Tel.: +86 27 87542618; fax: +86 27 87540724.
E-mail addresses: faw@hust.edu.cn, faw_73@163.com (A. Fan).
http://dx.doi.org/10.1016/j.ijhydene.2014.03.116

reported [7–17]. For instance, Maruta et al. [7,8] experimentally observed flame with repetitive extinction and ignition (FREI) in a 2-mm-diameter tube with a fixed temperature profile. Richecoeur and Kyritsis [9] observed the similar phenomenon for non-premixed methane/oxygen flame in a 4-mm-diameter curved duct. This combustion mode was later numerically captured by Jackson et al. [10]. Pizza et al. [11] investigated the dynamics of lean hydrogen/air flames in planar micro-channels by means of direct numerical simulation. They demonstrated five types of flames, including flame with periodic ignition and extinction, symmetric V-shaped flames, asymmetric flames, oscillating and pulsating flames and asymmetric flames. Kumar et al. [12,13] and Fan et al. [14–17] observed some special flame patterns in heated radial micro-channels, such as rotating spiral flame.

Tremendous contributions have been made to improve flame stability in micro- and meso-scale combustors. Thermal managements, such as heat recirculation and heat loss control, are good ways to compensate for the negative effect of heat loss and thus sustain stable flames in micro-scale devices. The "Swiss-roll" structure has been implemented to stabilize flames in micro- and meso-scale combustors [18–20]. Combustion characteristics of premixed H_2/air in a planar micro-combustor with stainless steel mesh was experimentally studied by Li et al. [21]. Their work showed that flame can be effectively anchored by the inserted porous media which led to a higher and uniform temperature distribution along the combustor wall. In addition, catalytic combustion is also an excellent way for stabilizing flame under small scales. Boyarko et al. [22] investigated catalytic combustion of H_2/O_2 mixture in platinum tubes with an internal diameter of 0.4 and 0.8 mm for micro-propulsion applications. Zhou et al. [23] studied catalytic micro-combustors made of different materials, i.e., quartz, alumina ceramic and copper. Their results manifested that the combustors' performances differ from each other due to their distinct reaction modes. Choi et al. [24] investigated combustion characteristics of a sub-millimeter catalytic combustor with platinum catalyst on porous ceramic. The results confirmed that the catalytic combustion is applicable to sub-millimeter scale combustors.

Utilizing the recirculation zone of flow field is another effective way to stabilize flame in micro-combustors. Yang et al. [25] developed three types of micro-combustors with or without a backward facing step. Their experiments showed that the step is very useful in controlling flame position and widening operational ranges of inlet velocity and H_2/air ratio. Khandelwal et al. [26] investigated flame stability of premixed CH_4/air in micro combustors with two backward steps. Their results demonstrated that stable flames can occur in multi-step-based micro combustors over wide ranges of inlet velocity and equivalent ratio. Wan et al. developed a micro-combustor with a bluff body [27] which can greatly expand the blow-off limit compared to the straight channel. Very recently, Fan et al. [28–30] comprehensively investigated the effects of dimension and shape of the bluff body and the solid material on the blow-off limit of this micro-combustor.

It is well known that cavity has been widely used for flame stabilization in supersonic combustion [31–33]. The main functions of cavities are to provide a low-velocity zone to stabilize flame and to extend the residence time of the fuel/air mixture and intermediate radicals. In the present work, we apply the wall cavities to anchor flame in a planar micro-channel and investigate the combustion characteristics of lean H_2/air mixture. Being limited by the size, it is very difficult to obtain information inside a micro-combustor by systematic experimental studies. On the other hand, numerical simulation provides a convenient and cost-effective approach to investigate micro-combustion phenomena and underlying mechanisms. Therefore, the aim of this work is to numerically study the effects of inlet velocity, length–depth ratio of the cavity, and equivalence ratio on combustion characteristics.

Numerical methods

Geometric model

The schematic diagram of the micro-combustor with wall cavities is shown in Fig. 1. The total length (L_0) is 18.0 mm and the distance from the left side wall of the cavity to the inlet (L_1) is 3 mm. The thicknesses of combustor walls (W_3) are 2 mm. The width (W_0) and height (W_1) of the combustor chamber are 10 mm and 1 mm, respectively. The angle between the cavity slope and horizontal is 45° (θ). The depth (W_2) of the cavities is 1 mm, while the length (L_2) takes the values of 1 mm, 2 mm and 3 mm, respectively. The length–depth ratio of the cavity is defined as $\xi = L_2/W_2$.

Mathematical model

Because the characteristic scale of the combustor chamber is still notably larger than the molecular mean-free path of the gases that flow through the micro-combustor, fluids can be reasonably treated as continuums. Therefore, the Navier–-Stokes equations are still applicable to the present study [34]. Our previous studies [27–30] and other researchers [19,35] indicated that turbulence models are better in predicting combustion characteristics than the laminar model. For example, Zhang et al. [35] reported that the turbulence model predicts the experimental data much better than the laminar model. Kuo and Ronney [19] also suggest that turbulence models more appropriately estimate the combustion characteristics in micro-combustors when the Reynolds number is

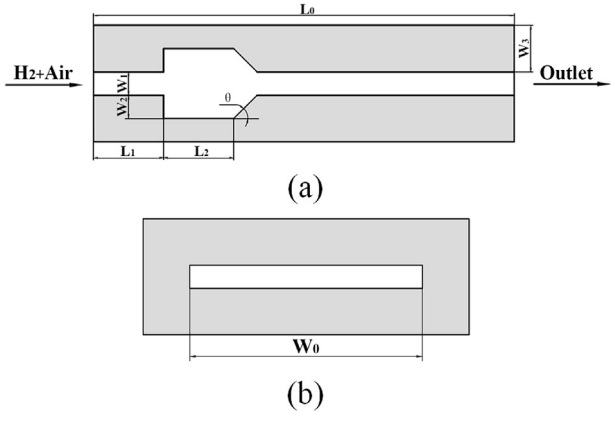

Fig. 1 – Schematic diagram of the micro combustor with cavities: (a) longitudinal cross section, (b) combustor exit.

above approximately 500. For the present combustor with cavities, the inlet velocity that corresponds to $Re = 500$ is approximately 8 m/s. The main purpose of the micro-combustor with cavities is to extend the upper limit of stable combustion, which is much larger than 8.0 m/s (refer to Section 3). In addition, we have compared all the turbulence models in our previous study [27–30] and found that the 'realizable *k-epsilon* model' is the best. Therefore, we adopt the 'realizable *k-epsilon* model' for the numerical simulation of the present work. The heat conduction in the solid walls is also considered in the computations.

Computation scheme

Hydrogen and air were selected as the fuel and oxidant, respectively. Quartz was used as the solid material. The density of the gas mixture was calculated using the ideal gas assumption, while the specific heat, viscosity and thermal conductivity were calculated from a mass fraction weighted average of the species' properties. The temperature dependences of thermal conductivity (λ) and specific heat capacity (c_p) of the solid material were incorporated using polynomial functions based on handbook values [36].

The reaction mechanism reported by Li et al. [37] was applied to model the combustion of H_2/air mixtures. It consists of 13 species and 19 reversible elementary reactions. The thermodynamic and transport properties of the gaseous species could be found in the up-to-date CHEMKIN databases [38] and other literature [39,40]. The surface reaction effect was not considered in the CFD simulation because the micro-combustor could be specially processed to ensure the inertness of all interior surfaces.

The boundary conditions are as follows. The uniform concentration and velocity distributions of the premixed mixture were specified at the inlet of the micro-combustor. The inlet temperature of mixture was set to 300 K. An outflow boundary condition was specified at the exit. A temperature of 1500 K, which is high enough to ignite the H_2/air mixture, was initialized for the fluid zone (this is called 'patch method' for ignition in the software Fluent). The effects of surface to surface radiation between the inner surfaces of the combustor were considered using the discrete ordinates (DO) model [19]. At the outer surfaces of solid walls, the total heat loss via both natural convection and thermal radiation to the surroundings was calculated using Eq. (1):

$$q = h(T_{W,O} - T_\infty) + \varepsilon\sigma\left(T_{W,O}^4 - T_\infty^4\right) \quad (1)$$

where h is the natural convection heat transfer coefficient (20 W/(m^2 K)) [41], $T_{w,o}$ is the outer wall temperature, T_∞ is the ambient temperature (300 K), ε is the emissivity of the solid surface with a value of 0.92, and σ is the Stephan–Boltzmann constant, 5.67×10^{-8} W/(m^2 K^4).

The computational fluid dynamics (CFD) software package FLUENT 6.3 [42] was applied to solve the mass, momentum, energy and species conservation equations as well as the conjugated heat conduction in solid walls. The second-order upwind scheme was used to discretize the model, and the "SIMPLE" algorithm was employed to couple the pressure and velocity. Because the aspect ratio (W_0/W_1) of the combustor chamber is very large (10:1), we adopted a 2-dimensional model for our numerical simulations to reduce the computation load. Accuracy of the 2-dimensional model has been validated in our previous work [27–30]. The results were verified to be grid-independent, and a non-uniform square grid system was employed in the computation. The finest grid size is 0.02 mm and the total grid numbers for $\xi = 1$, 2 and 3 are 125333, 131683 and 138033, respectively. The convergence of the CFD simulation was judged based on the residuals of all governing equations. The results obtained in this study were achieved with residuals smaller than 1.0×10^{-6}. When convergence reached, the conversion rate of hydrogen was calculated through Eq. (2):

$$\eta = 1 - \frac{C_{out}}{C_{in}} \quad (2)$$

where C_{in} and C_{out} are hydrogen mass fractions at the inlet and outlet of the micro-combustor, respectively.

Results and discussions

Model validation

To validate the accuracy of the numerical model, we measured the exhausted gas temperature of the combustor with a length–depth ratio of 3 at the equivalence ratio of 0.3. A K-type thermocouple was placed at the center of combustor exit to measure the exhaust gas temperature, and the temperature presented in this paper has been corrected considering the heat losses to the ambient [43]. The details of the experimental system and method could be found elsewhere [27]. The experimental data and numerical results were compared, as shown in Fig. 2. It is seen from Fig. 2 that the differences between the experimental data and numerical results are not so big, especially at large inlet velocities. The maximum relative error is around 10.3% which occurs at the inlet velocity of 8 m/s, while for $V_{in} = 26$ m/s, the relative error is only around 4.43%. This confirms the reasonable accuracy

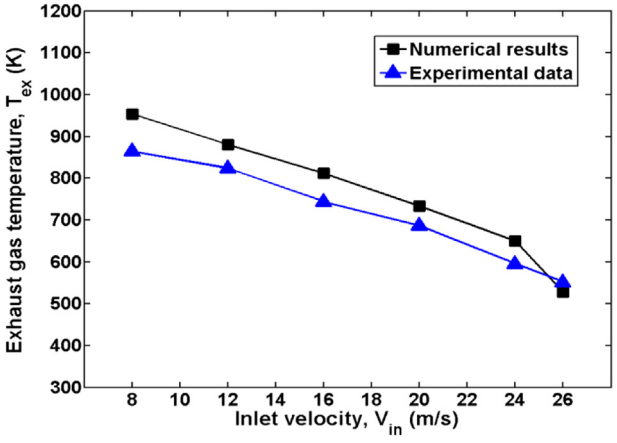

Fig. 2 – Comparison between experimental data and numerical results of the exhaust gas temperature at the equivalence ratio of 0.3. The length–depth ratio of cavities is 3.

of the numerical model adopted in the present paper, especially at high inlet velocities.

Effects of inlet velocity on combustion characteristics

In this section, we discuss the effect of inlet velocity on combustion characteristics. The length–depth ratio of the cavities is 3 and the equivalence ratio is 0.4. Fig. 3 shows the mass fraction contours of radical OH which was often used to indicate the location of reaction zone. From Fig. 3, it is seen that when the inlet velocity is relatively low (e.g., $V_{in} = 8$ m/s), the reaction zone is mainly located in the two cavities due to the formation of low velocity regions. It implies that the cavities act as flame holders and the flame is effectively anchored by them. However, it is noted that, other than the major reaction zone, there also exist a thinner one behind the cavity. This reaction zone is stabilized by the boundary layer which is also a region with low velocity. Another characteristic of this case is that the upper and lower reaction zones merge at the center of the downstream channel. However, with the increase of the inlet velocity, the lengths of the boundary stabilized reaction zones grow longer and the merging location of the upper and lower ones is accordingly postponed, as shown in Fig. 3b and c. Finally, the upper and lower reaction zones split completely at a large enough inlet velocity, as clearly illustrated in Fig. 3d. In addition, Fig. 3d shows that on each side of the combustor chamber, the cavity stabilized reaction zone and the boundary stabilized reaction zone are separated from each other.

Fig. 4 shows the temperature fields at different inlet velocities. Comparing Fig. 4 with Fig. 3, we see that the variation of high temperature regions is consistent with that of the reaction zones. For instance, when the inlet velocity is 8 m/s, the high temperature region is mainly located in the cavities, as well as the boundaries and inner walls that right behind the cavities. As the inlet velocity is increased, the second high temperature region that corresponds to the boundary stabilized reaction zone is pushed farther downstream (see Fig. 4b and c). Especially, these two high temperature regions will be separated from each other at sufficiently high inlet velocity, as shown in Fig. 4d.

The variation of high temperature region has a direct influence on the outer wall temperature profile, as shown in Fig. 5. When the inlet velocity is 8 m/s, the highest wall

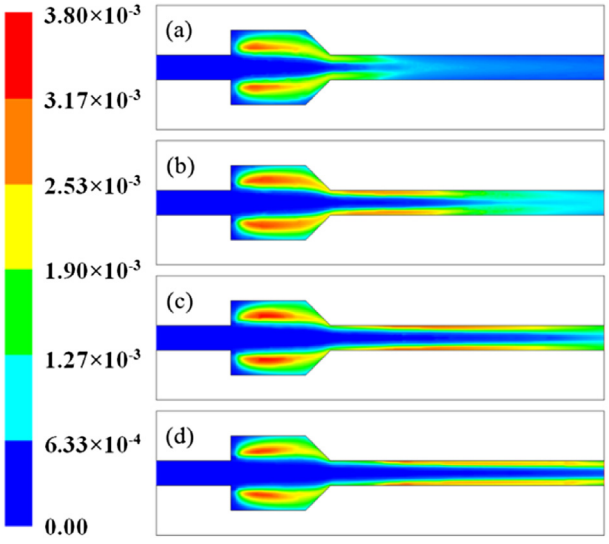

Fig. 3 – Mass fraction contours of OH at different inlet velocities: (a) $V_{in} = 8$ m/s, (b) $V_{in} = 16$ m/s, (c) $V_{in} = 24$ m/s, (d) $V_{in} = 32$ m/s. The length–depth ratio of cavities is 3 and the equivalence ratio is 0.4.

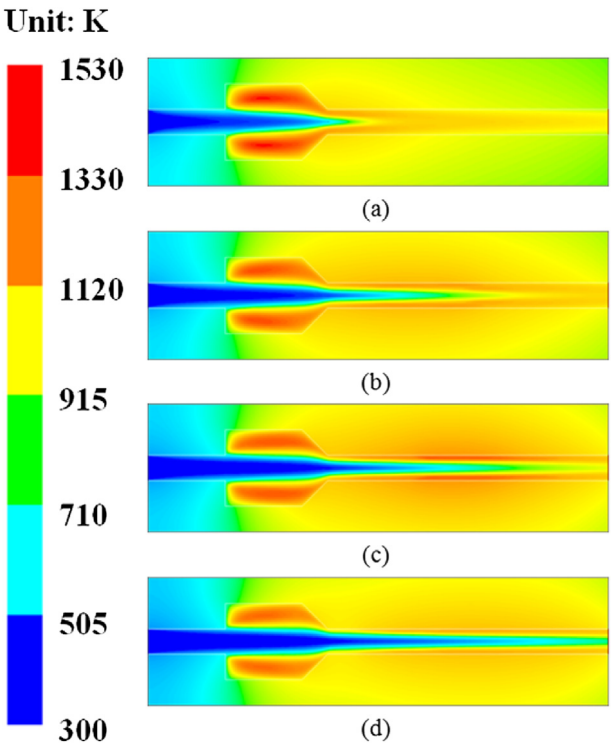

Fig. 4 – Temperature field at different inlet velocities: (a) $V_{in} = 8$ m/s, (b) $V_{in} = 16$ m/s, (c) $V_{in} = 24$ m/s, (d) $V_{in} = 32$ m/s. The length–depth ratio of cavities is 3 and the equivalence ratio is 0.4.

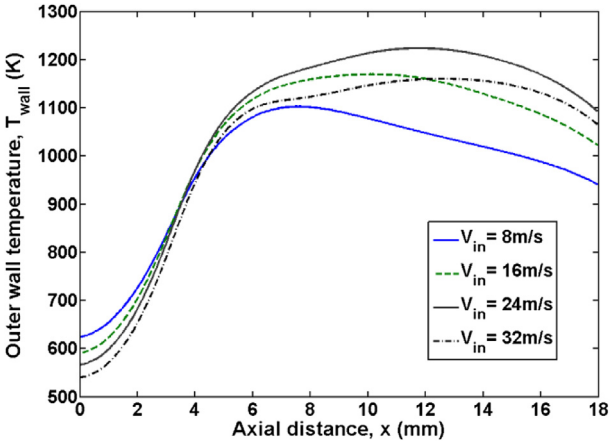

Fig. 5 – Outer wall temperature profiles at different inlet velocities. The length–depth ratio of cavities is 3 and the equivalence ratio is 0.4.

temperature appears at the location corresponding to the middle of the cavity, and then descends due to the heat losses from the outer wall. As the inlet velocity is increased to 16 m/s, the wall temperature of the midstream and downstream grows higher, while the upstream wall temperature slightly decreases. The reasons for these phenomena lie in two aspects. On one hand, a large inlet velocity means more fuel supply and more heat release. On the other hand, the reaction zone will be pushed farther downstream and the upstream inner walls will be more strongly cooled by the fresh cold mixture. When the inlet velocity is further increased, a slight valley appears in the outer wall temperature profile (see Fig. 5). This is consistent with temperature field shown in Fig. 4d which is caused by the separation of the cavity stabilized reaction zone and the boundary stabilized reaction zone.

According to the variation of the reaction zone, the combustion completeness of the fuel gas (H_2) will also change with the inlet velocity. Fig. 6 shows the mass fraction of H_2 along the vertical direction of the combustor exit for different inlet velocities. It is clearly seen that when the inlet velocity is relatively low (e.g., V_{in} = 8 m/s and 16 m/s), the hydrogen fuel is almost completely consumed in the combustion process. With the increase of the inlet velocity, the unconsumed hydrogen exhibits a sharp peak at the middle of the combustor exit, which can be clearly seen from the case of V_{in} = 32 m/s. For the sake of comparison, we define a 'flame-splitting limit' as the largest inlet velocity when the unconsumed hydrogen mass fraction reaches 20%. For the present case, the flame-splitting limit is around 32 m/s. To more clearly show this variation tendency, we provided hydrogen concentration distribution (H_2 mass fraction contours) in Fig. 7. It is noted that when the inlet velocity is 8 m/s, the fuel is almost completely consumed at the exit of the cavities. As the inlet velocity is raised to 16 m/s, the hydrogen fuel need a longer distance to be burned, but can also fully converted before leaving the combustor exit. When the inlet velocity is 24 m/s, hydrogen cannot be completely consumed until the end of the channel. As the inlet velocity is increased up 32 m/s, large amount of hydrogen leaks from the combustor exit, i.e., flame splitting appears, as clearly shown in Fig. 7d.

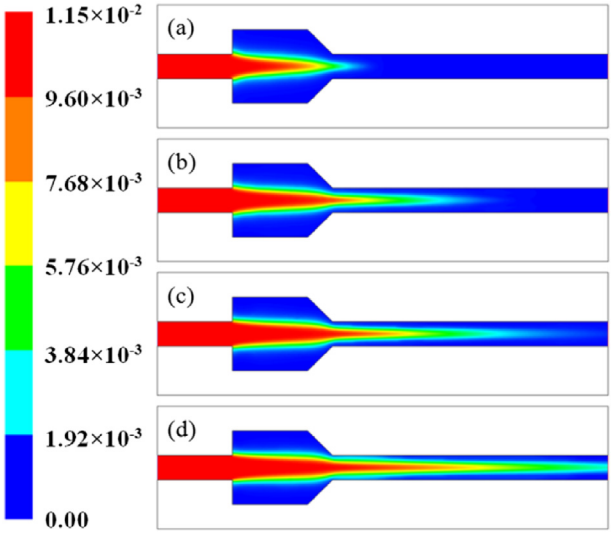

Fig. 7 – Mass fraction contours of H_2 at different inlet velocities: (a) V_{in} = 8 m/s, (b) V_{in} = 16 m/s, (c) V_{in} = 24 m/s, (d) V_{in} = 32 m/s. The length–depth ratio of cavities is 3 and the equivalence ratio is 0.4.

Fig. 8 illustrates the variation of conversion rate of hydrogen with the inlet mixture velocity. It is seen from this figure that the maximum efficiency (nearly 100%) occurs at the inlet velocity of around 10 m/s. For cases with a lower inlet velocity (e.g., V_{in} = 8 m/s), the conversion rate slightly decreases but still remains at above 99%. When the inlet velocity is increased from 10 m/s, the conversion rate decreases first slowly and then drops with an acceleration. For instance, the conversion rate of hydrogen decreases from 97.98% to 80.36% as the inlet velocity is raised from 20 m/s to 32 m/s. This is due to the flame splitting phenomenon which leads to large amount of fuel leakage as discussed above. In addition, increasing the inlet velocity leads to a shorter residence time, which is detrimental for a complete reaction.

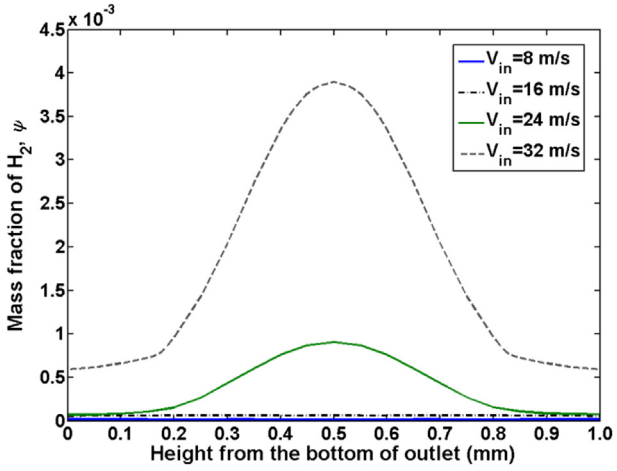

Fig. 6 – Mass fraction of H_2 at the combustor exit for different inlet velocities. The length–depth ratio of cavities is 3 and the equivalence ratio is 0.4.

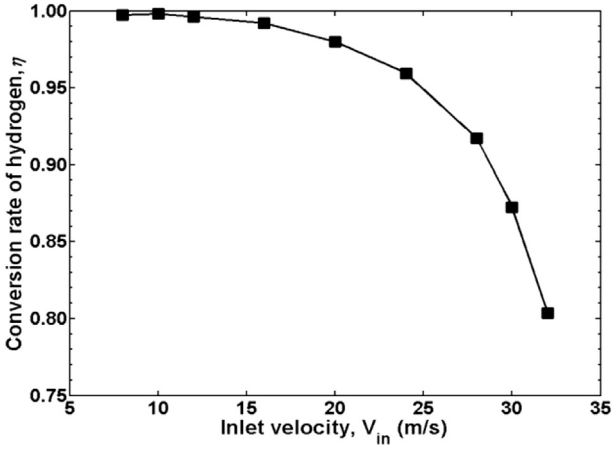

Fig. 8 – Variation of conversion rate of hydrogen with the inlet velocity. The length–depth ratio of cavities is 3 and the equivalence ratio is 0.4.

Effects of equivalence ratio

In this section we investigate the effect of equivalence ratio on the combustion characteristics. The length–depth ratio of the cavities is 3 and the inlet velocity is fixed at 10 m/s. Fig. 9 depicts the OH mass fraction contours for different equivalence ratios. It is clearly observed that the OH concentration increases with the equivalence ratio, which represents a more intensive chemical reaction and a larger heat release at a higher equivalence ratio. This can also be reflected by the temperature fields as shown in Fig. 10. From Fig. 10, the temperature level in the cavities and downstream channel rises with the increase of the equivalence ratio. More importantly, it is noted from Fig. 9 that the location where the upper and lower reaction zones merge shifts upstream at a higher equivalence ratio (e.g., $\phi = 0.5$). This is because that the burning velocity is larger for a bigger equivalence ratio. Thus, flame can be stabilized at a comparatively upstream location, which is clearly demonstrated in the H_2 mass fraction contours for different equivalence ratios (see Fig. 11). This implies that a larger flame-splitting limit can be achieved at a higher equivalence ratio. Fig. 12 shows that the corresponding flame-splitting limits for equivalence ratio of 0.3, 0.4 and 0.5 are 26 m/s, 32 m/s and 45 m/s, respectively.

The numerical results also show that the equivalence ratio has a negligible impact on the conversion rate of hydrogen at low inlet velocity, but its effect becomes significant at high inlet velocity. Here, we give two examples for comparison. When the inlet velocity is 10 m/s, all the conversion rate of hydrogen at different equivalence ratios (0.3, 0.4 and 0.5) are all very high (>99.3%). However, at the inlet velocity of 24 m/s, the conversion rate of hydrogen is 84.87%, 95.94% and 99.14% for the equivalence ratio of 0.3, 0.4 and 0.5, respectively.

Effects of the length–depth ratio of cavity

In this section, we examine the effect of the length–depth ratio of cavities on the combustion characteristics, especially on the flame-splitting limit. The equivalence ratio is selected to be 0.4 and the inlet mixture velocity is fixed at 10 m/s. Fig. 13 shows the flame-splitting limit for different length–depth ratios ($\xi = 1, 2, 3$, corresponding to a cavity length (L_2) of 1 mm, 2 mm and 3 mm, respectively). From this figure it is known that the corresponding limits for $\xi = 1$, 2 and 3 are 18 m/s, 27 m/s and 32 m/s, respectively. This indicates that for $\xi = 1$ it has a splitting limit which is only slightly larger than half the value for $\xi = 3$. Nevertheless, the flame-splitting limit of $\xi = 1$ is still three times the blow-off limit of the corresponding straight channel, which demonstrates that the flame stability is appreciably strengthened by the wall cavities.

To elucidate the flame stabilization mechanism of the cavities, we present the contours of the longitudinal velocity component in the local region near the cavities (0.002 m ≤ x ≤ 0.008 m, 0.0008 m ≤ y ≤ 0.0042 m), as shown in Fig. 14. Here, the recirculation zone is defined as the region

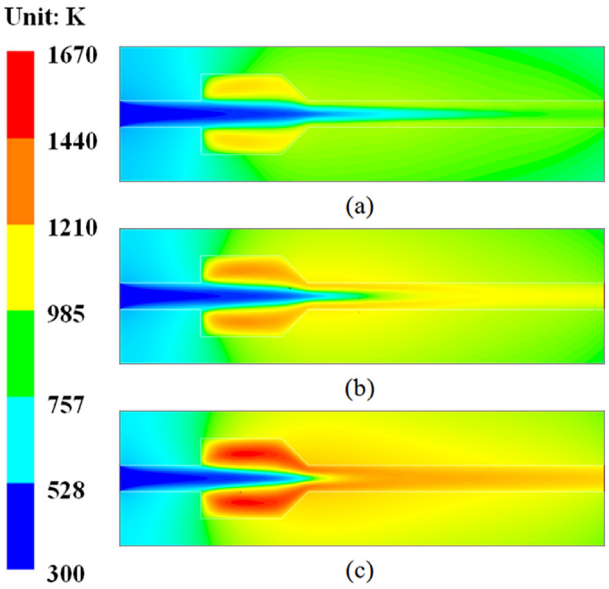

Fig. 10 – Temperature field at different equivalence ratios. The length–depth ratio of cavities is 3 and the inlet mixture velocity is 10 m/s.

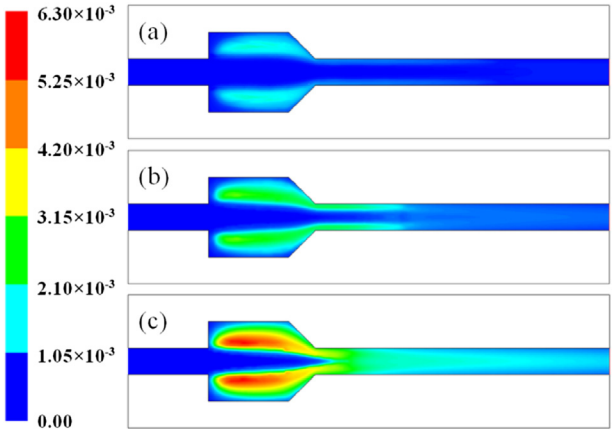

Fig. 9 – OH mass fraction contours at different equivalence ratios: (a) $\phi = 0.3$, (b) $\phi = 0.4$, (c) $\phi = 0.5$. The length–depth ratio of cavities is 3 and the inlet mixture velocity is 10 m/s.

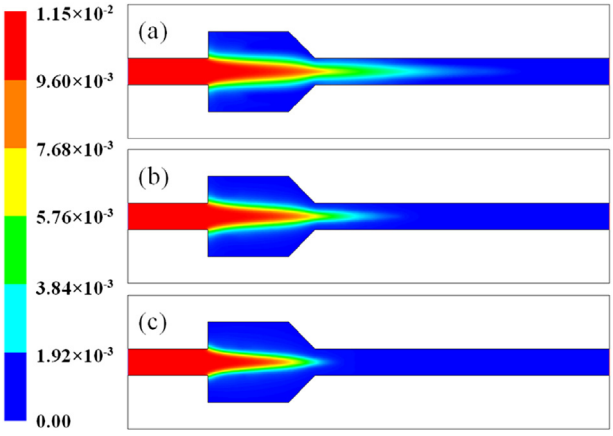

Fig. 11 – H_2 mass fraction contours at different equivalence ratios: (a) $\phi = 0.3$, (b) $\phi = 0.4$, (c) $\phi = 0.5$. The length–depth ratio of cavities is 3 and the inlet velocity is 10 m/s.

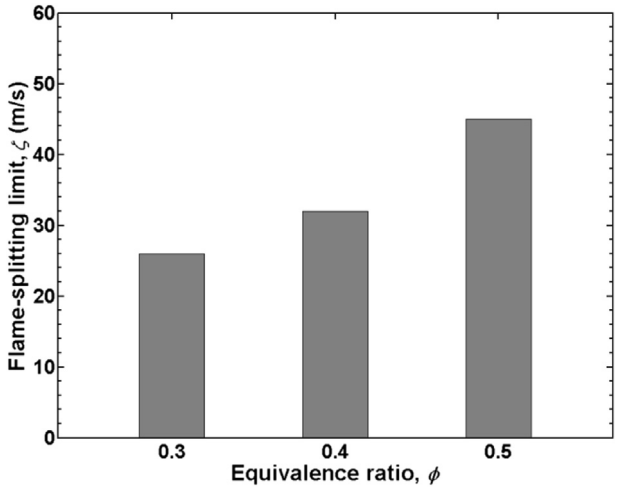

Fig. 12 – Flame splitting limits at different equivalence ratios. The length–depth ratio of cavities is 3 for all cases.

where the longitudinal velocity component is less than zero. In addition, the region where the longitudinal velocity component is between zero and 10 m/s is referred to as the low velocity zone. From Fig. 14, it is noted that the recirculation zones of the three cases are almost of the same size, but the area of low velocity zone increases with the length–depth ratio of cavities. Thus, when the cavity length increases, the reaction zone area also increases. As a result, the fuel has more sufficient time to be burned and a higher conversion rate of hydrogen can be achieved, which is advantageous for a larger 'flame splitting limit'. On the other hand, due to the more complete combustion in the cavity, more obvious gas expansion and higher longitudinal velocity were noted at the cavity exit as the cavity length increases (Fig. 14), which is detrimental for a larger 'flame splitting limit'. However, this negative effect is overwhelmed by the positive aspect of a longer cavity. In conclusion, a larger length–depth ratio leads to a larger 'flame splitting limit'.

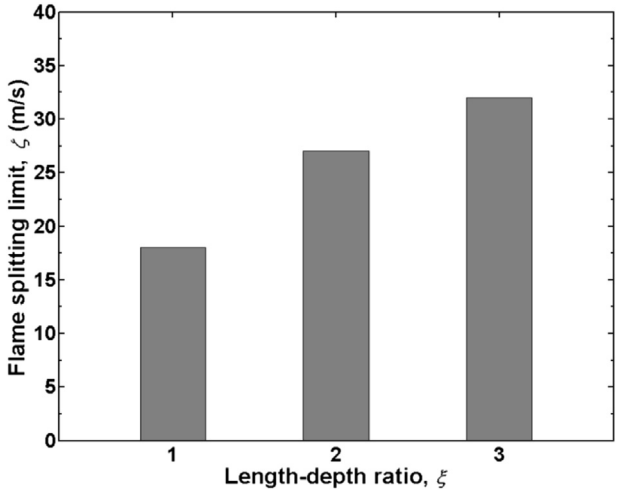

Fig. 13 – Flame splitting limit at the equivalence ratio of 0.4 for different length–depth ratios of cavities.

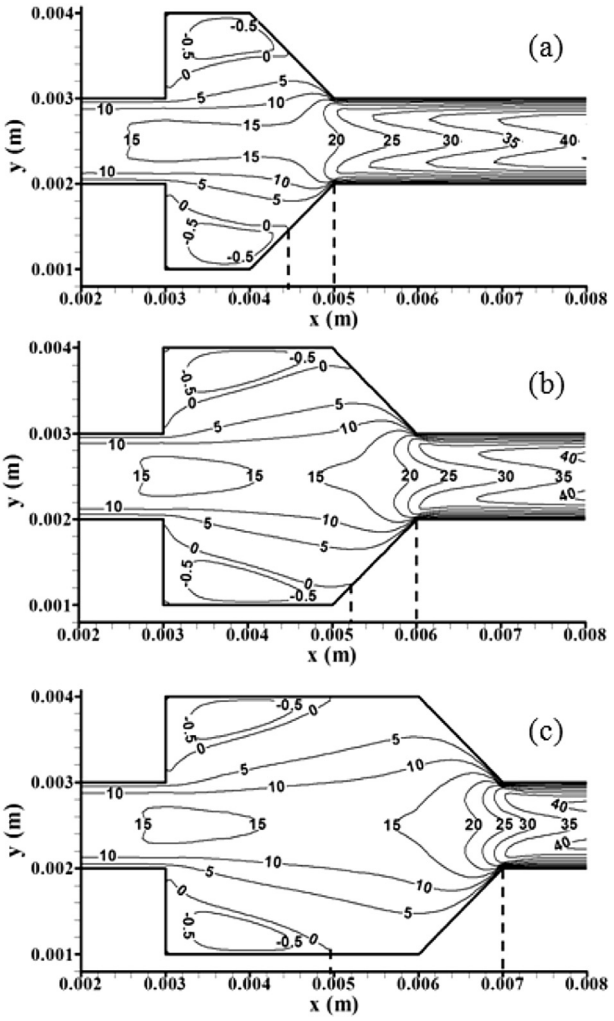

Fig. 14 – Contours of the longitudinal velocity component in the region near the cavities with different length–depth ratios: (a) $\xi = 1$, (b) $\xi = 2$, (c) $\xi = 3$. The equivalence ratio is 0.4 and the inlet velocity is 10 m/s.

Although a bigger length–depth ratio of the cavities leads to a larger flame-splitting limit, this does not mean that it benefits the combustor performances on all aspects. For example, we plotted the outer wall temperature profile for different length–depth ratios in Fig. 15. From this figure one can see that the wall temperature level declines with the increase of the length–depth ratio. In other word, the outer wall temperature for $\xi = 3$ is the lowest among the three cases. Specifically, there are three regions that demonstrate obvious temperature differences. The first region is that near the cavity, where the peak temperatures of the three cases are 1175 K, 1138 K, and 1130 K, respectively. The second region is near the entrance of the combustor where relatively obvious temperature differences are observed. This is because the outer wall of cavity is thinner than elsewhere and the thermal resistance in the horizontal direction is increased. Therefore, less heat is conducted upstream via the thinner solid wall with a larger length–depth ratio. The third region is the wall located downstream of the cavity. The corresponding outer

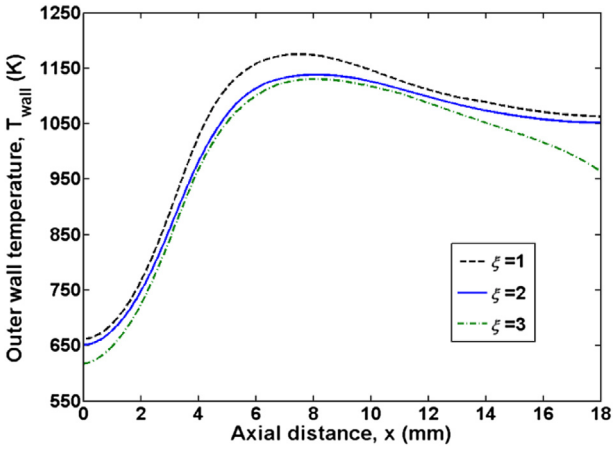

Fig. 15 – Outer wall temperature profiles at different length–depth ratios of cavities: (a) $\xi = 1$, (b) $\xi = 2$, (c) $\xi = 3$. The equivalence ratio is 0.4 and the inlet velocity is 10 m/s.

wall temperatures at the combustor exit for $\xi = 1$, 2 and 3 are 1063 K, 1052 K and 963 K, respectively. This is because more fuel has been consumed in the cavities with a larger length–depth ratio and less heat is released in the downstream. Therefore, an even larger length–ratio of the cavity is not beneficial for this type of micro combustors if the combustor walls are used as heat sources for thermoelectric or thermophotovoltaic devices, which requires a sufficiently high temperature level of the outer walls as well as a wide operational range.

Conclusions

The combustion characteristics of premixed H_2/air flame in a micro-combustor with wall cavities were numerically investigated with detailed chemistry. Concentration was focused on the effects of inlet velocity, equivalence ratio, and the length–depth ratio of the cavity. The results reveal that there are two mechanisms which responsible for the flame stabilization. The major one is the recirculation zone and low velocity zone that formed in the cavity, while the other one is the ordinary flame stabilization mechanism for a flow reactor, i.e., boundary layer of the inner wall. Moreover, it is shown that with the increase of inlet velocity, the flame front splits in the middle which leads to a large amount of unconsumed fuel leakage from the combustor exit. Furthermore, the conversion rate of hydrogen first slightly rises and then descends at an increasing rate with the increase of the inlet velocity. In addition, the flame-splitting limit is extended at a higher equivalence ratio. This is mainly due to the larger burning velocity when fuel concentration is higher. Finally, it is demonstrated that the flame-splitting limit increases but the wall temperature level decreases for a larger length–depth ratio of cavity. Thus, in order to ensure a sufficiently high temperature level of the outer walls and a wide operational range, a length–depth ratio of 3 is recommended for the application of micro-combustors with wall cavities.

Acknowledgments

This work was supported by: 1) National Basic Research Program of China (Grant No. 2014CB239600), 2) National Natural Science Foundation of China (Grant Nos. 51276073, 51336010), 3) Fundamental Research Funds for the Central Universities (HUST2013QN077), and 4) Foundation of Key Laboratory of Low-grade Energy Utilization Technologies and Systems, Chongqing University, China.

REFERENCES

[1] Fernandez-Pello AC. Micro-power generation using combustion: issues and approaches. Proc Combust Inst 2002;29:883–99.
[2] Sirignano WA, Pham TK, Dunn-Rankin D. Miniature-scale liquid-fuel-film combustor. Proc Combust Inst 2002;29:925–31.
[3] Zamaschikov VV. Combustion of gases in thin-walled small diameter tubes. Combust Explos Shock Waves 1995;131:10–6.
[4] Maruta K. Micro and mesoscale combustion. Proc Combust Inst 2011;33:125–50.
[5] Wang HO, Luo K, Lu SQ, Fan JR. Direct numerical simulation and analysis of a hydrogen/air swirling premixed flame in a micro combustor. Int J Hydrogen Energy 2011;36:3838–49.
[6] Bedra L, Rutigliano M, Balat-Pichelin M, Cacciatore M. Atomic oxygen recombination on quartz at high temperature: experiments and molecular dynamics simulation. Langmuir 2006;22:7208–16.
[7] Maruta K, Kataoka T, Kim NI, Minaev S, Fursenko R. Characteristics of combustion in a narrow channel with a temperature gradient. Proc Combust Inst 2005;30:2429–36.
[8] Fan AW, Minaev S, Sereshchenko E, Tsuboi Y, Oshibe H, Nakamura H, et al. Propagation dynamics of splitting flames in a heated microchannel. Combust Explos Shock Waves 2009;45:245–50.
[9] Richecoeur F, Kyritsis DC. Experimental study of flame stabilization in low Reynolds and Dean number flows in curved mesoscale ducts. Proc Combust Inst 2005;30:2419–27.
[10] Jackson TL, Buckmaster J, Lu Z, Kyritsis DC, Massa L. Flames in narrow circular tubes. Proc Combust Inst 2007;31:955–62.
[11] Pizza G, Frouzakis CE, Mantzaras J, Tomboulides AG, Boulouchos K. Dynamics of premixed hydrogen/air flames in microchannels. Combust Flame 2008;152:433–50.
[12] Kumar S, Maruta K, Minaev S. Pattern formation of flames in radial microchannels with lean methane-air mixtures. Phys Rev E 2007;75:016208.
[13] Kumar S, Maruta K, Minaev S. On the formation of multiple rotating Pelton-like flame structures in radial microchannels with lean methane-air mixtures. Proc Combust Inst 2007;31:3261–8.
[14] Fan AW, Minaev S, Kumar S, Liu W, Maruta K. Experimental study on flame pattern formation and combustion completeness in a radial microchannel. J Micromech Microengin 2007;17:2398–406.
[15] Fan AW, Maruta K, Nakamura H, Kumar S, Liu W. Experimental investigation on flame pattern formations of DME-air mixtures in a radial microchannel. Combust Flame 2010;157:1637–42.
[16] Fan AW, Nakamura H, Maruta K, Liu W. Experimental investigation of flame pattern transitions in a heated radial micro-channel. Appl Therm Eng 2012;47:111–8.

[17] Fan AW, Wan JL, Maruta K, Nakamura H, Yao H, Liu W. Flame dynamics in a heated meso-scale radial channel. Proc Combust Inst 2013;34:3351–9.
[18] Sitzki L, Borer K, Wussow S, Schuster E, Maruta K, Ronney PD, et al. Combustion in microscale heat-recirculating burners. In: AIAA-2001-1078, 38th AIAA space sciences & exhibit, Reno, NV.
[19] Kuo CH, Ronney PD. Numerical modeling of non-adiabatic heat-recirculating combustors. Proc Combust Inst 2007;31:3277–84.
[20] Kim NI, Kato S, Kataoka T, Yokomori T, Maruyama S, Fujimori T, et al. Flame stabilization and emission of small Swiss-roll combustors as heaters. Combust Flame 2005;141:229–40.
[21] Li J, Chou SK, Li ZW, Yang WM. Experimental investigation of porous media combustion in a planar micro-combustor. Fuel 2010;89:708–15.
[22] Boyarko GA, Sung CJ, Schneider SJ. Catalyzed combustion of hydrogen-oxygen in platinum tubes for micro-propulsion applications. Proc Combust Inst 2005;30:2481–8.
[23] Zhou JH, Wang Y, Yang WJ, Liu JZ, Wang ZH, Cen KF. Combustion of hydrogen-air in catalytic micro-combustors made of different material. Int J Hydrogen Energy 2009;34:3535–45.
[24] Choi WY, Kwon SJ, Shin H. Combustion characteristics of hydrogen-air premixed gas in a sub-millimeter scale catalytic combustor. Int J Hydrogen Energy 2008;33:2400–8.
[25] Yang WM, Chou SK, Shu C, Li ZW, Xue H. Combustion in micro-cylindrical combustors with and without a backward facing step. Appl Therm Eng 2002;22:1777–87.
[26] Khandelwal B, Sahota GPS, Kumar S. Investigations into the flame stability limits in a backward step micro scale combustor with premixed methane-air mixtures. J Micromech Microengin 2010;20:095030.
[27] Wan JL, Fan AW, Maruta K, Yao H, Liu W. Experimental and numerical investigation on combustion characteristics of premixed hydrogen/air flame in a micro-combustor with a bluff body. Int J Hydrogen Energy 2012;37:19190–7.
[28] Fan AW, Wan JL, Liu Y, Pi BM, Yao H, Maruta K, et al. The effect of the blockage ratio on the blow-off limit of a hydrogen/air flame in a planar micro-combustor with a bluff body. Int J Hydrogen Energy 2013;38:11438–45.
[29] Fan AW, Wan JL, Maruta K, Yao H, Liu W. Interactions between heat transfer, flow field and flame stabilization in a micro-combustor with a bluff body. Int J Heat Mass Trans 2013;66:72–9.
[30] Fan AW, Wan JL, Liu Y, Yao H, Liu W. Effect of bluff body shape on the blow-off limit of hydrogen/air flame in a planar micro-combustor. Appl Therm Eng 2014;62:13–9.
[31] Kim KM, Baek SW, Han CY. Numerical study on supersonic combustion with cavity-based fuel injection. Int J Heat Mass Trans 2004;47:271–86.
[32] Rasmussen CC, Driscoll JF, Hsu KY, Doubar JM, Gruber MR, Carter CD. Stability limits of cavity-stabilized flames in supersonic flow. Proc Combust Inst 2005;30:2825–33.
[33] Sun MB, Wu HY, Fan ZQ, Wang HB, Bai XS, Wang ZG, et al. Flame stabilization in a supersonic combustor with hydrogen injection upstream of cavity flame holders: experiments and simulations. J Aerosp Eng 2011;225:1351–65.
[34] Beskok A, Karniadakis GE. A model for flows in channels, pipes, and ducts at micro and nano scales. Microscale Therm Eng 1999;3:43–77.
[35] Zhang YS, Zhou JH, Yang WJ, Liu MS, Cen KF. Study on the model selection for micro-combustion simulation. Proc Chin Soc Elect Eng 2006;26:81–7 [in Chinese].
[36] Ma QF, Fang RS, Xiang LC. Handbook of thermo-physical properties. Bejing: China Agricultural Machinery Press; 1986 [in Chinese].
[37] Li J, Zhao ZW, Kazakov A, Dryer FL. An updated comprehensive kinetic model of hydrogen combustion. Int J Chem Kinet 2004;36:1–10.
[38] CHEMKIN-PRO Release 15101. San Diego, CA: Reaction Design Inc.; 2010.
[39] Capitelli M, Gorse C, Longo S, Giordano D. Collision integrals of high-temperature air species. J Thermophys Heat Transf 2000;14:259–68.
[40] Laricchiuta A, Bruno D, Capitelli M, Catalfamo C, Celiberto R, Colonna G, et al. High temperature Mars atmosphere, part I: transport cross sections. Eur Phys J D 2009;54:607–12.
[41] Holman JP. Heat transfer. 9th ed. New York: McGraw-Hill; 2002.
[42] Fluent 6.3 user's guide. Lebanon: New Hampshire: Fluent Inc.; 2006.
[43] Brundage AL, Donaldson AB, Gill W, Kearney SP, Nicolette VF, Yilmaz N. Thermocouple response in fires, part 1: considerations in flame temperature measurements by a thermocouple. J Fire Sci 2011;29:195–211.